ADVANCED OPTICAL MATERIALS
www.advopticalmat.de

Multi-Spectral Materials: Hybridisation of Optical Plasmonic Filters and a Terahertz Metamaterial Absorber

*Iain J. H. McCrindle, James Grant, Timothy D. Drysdale, and David R. S. Cumming**

Multi-spectral imagers can combine several spectrally specific cameras into a single system. It is also possible to use image fusion algorithms to provide a composite image of a scene over several wavebands. A single image that combines data from multiple wavebands can convey more information than individual images at each wavelength.[1–4] The diversity of materials required for imaging separate spectral bands mean that current wide-band multi-spectral imaging systems must use a range of different cameras. For example, a common digital camera uses silicon photodiodes as part of a complementary metal-oxide semiconductor (CMOS) chip, whereas an IR detector requires a different semiconductor material, such as indium antimonide (InSb), to act as a photodiode.[5] IR imagers can also be made with microbolometer arrays utilising materials such as vanadium oxide (VOx).[6] VOx has also demonstrated potential at terahertz (THz) frequencies[7] and through integration with a THz metamaterial (MM) absorber, has been optimised for THz imaging.[8] Further spectral selectivity within specific wavebands can also be desirable in applications such as optical imaging, where dye doped colour filters are often used in conjunction with photodiodes to form a full colour image of a scene.

Work to date has shown the potential for co-integration of different wavebands on a single chip.[9,10] However, because the different wavelength sensors are not coaxial, the visible/IR and THz wavebands must be detected using different regions on the surface of the chip. We propose the use of a synthetic multi-spectral material (SMM): a single structured material capable of operating over different wavebands simultaneously, thereby maximising the spectral information density of a multi-spectral imager in a coaxial format. SMMs exploit hybridised plasmonic and MM structures to combine multi-spectral functionalities into a single material.[11d]

Surface plasmons (SP) are electron density oscillations at the interface between a conductor and a dielectric. SPs can resonantly couple with incident light to form surface plasmon polaritons (SPP) in a process known as surface plasmon resonance (SPR). Periodic subwavelength hole arrays, at optical wavelengths, etched into a thin metal film can excite SPR leading to enhanced transmission and wavelength filtering of the incident light.[12–15] Colour filters have been fabricated by etching triangular subwavelength hole arrays of varying periods and hole sizes into a 150 nm aluminium film, sandwiched between two silicon dioxide layers.[16,17] Plasmonic filters have been optimised for digital imaging by engineering transmission spectra corresponding to the 1931 International Commission on Illumination (CIE) colour matching functions[18] and have also been integrated with CMOS image sensors.[19,20] Filters fabricated into a metal layer as part of the CMOS process offer a solution to substantial cross-talk between different colours that is expected as CMOS imagers scale to smaller sizes.[21,22] It is also possible to extend the operation of plasmonic filters to near IR (NIR) wavelengths by further scaling of the hole size and period.[11]

At THz frequencies the plasmonic response is diminished due to the high conductivity of the metal, however, a MM with a specific unit cell geometry can still exhibit resonant behaviour.[23–26] A MM absorber consists of a metal ground plane and an electric ring resonator (ERR) array, separated by a dielectric spacer. The ERR couples to the incident electric field and magnetic coupling is provided by the inclusion of a ground plane, as can be observed by anti-parallel currents on the metal surfaces.[27–32] At resonance, absorption is maximised by matching the wave impedance of the MM to the wave impedance of free space and engineering a large extinction coefficient.[28–30]

Our SMM consists of plasmonic filters fabricated into the ground plane of a THz MM absorber, which uses a hollow cross shaped ERR. The SMM is capable of filtering fifteen optical wavelengths and a NIR wavelength whilst simultaneously absorbing a single THz frequency through exploitation of two unique electromagnetic phenomena. The sparseness of high performance THz detectors means that it is advantageous to include the THz detection medium as part of the SMM. Hybridisation of the MM absorber with plasmonic filters yields a significant advancement towards the creation of a coaxial multi-spectral imager operating in visible, NIR and THz wavelength regimes.

The SMM geometry, layer structure and composition were optimised by performing simulations using Lumerical FDTD Solutions.[33] The plasmonic filter structures are significantly smaller than the MM absorber features and required a very fine mesh to define the holes. The small mesh resulted in a substantial increase in memory requirements compared with a standalone MM absorber, such that it was impractical to simulate the complete SMM structure at THz frequencies. However, it is possible to consider the ground plane of the SMM as an unperforated metal film at THz frequencies.[11] Optimisation of the entire SMM was performed by independently simulating the plasmonic filters and the MM absorber, with an unperforated ground plane. Details of the simulation procedures are outlined in the experimental section.

The resonant wavelength, λ_{SPP}, for a plasmonic filter triangular hole array is given by Equation (1):

I. J. H. McCrindle, Dr. J. Grant,
Dr. T. D. Drysdale, Prof. D. R. S. Cumming
Microsystems Technology Group
School of Engineering
University of Glasgow
G12 8LT, UK
E-mail: david.cumming.2@glasgow.ac.uk

DOI: 10.1002/adom.201300408

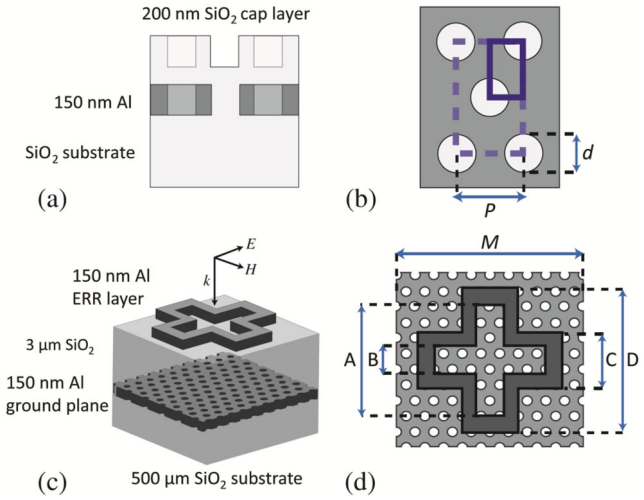

Figure 1. Plasmonic filter nanohole array illustrations and synthetic multi-spectral material (SMM) illustrations. (a) Cross section illustration of a plasmonic filter. (b) Illustration of the simulated plasmonic filter structure. The simulation region is surrounded by the solid purple box and the dashed black line encloses the unit cell of the triangular hole array. *P* denotes the hole period and *d* denotes the hole diameter. (c) SMM layer structure showing a single metamaterial (MM) absorber unit cell. Field orientations are also shown. (d) Top down schematic of the SMM showing the electric ring resonator (ERR) geometry. *M* denotes the period of the MM absorber unit cell.

$$\lambda_{SPP} = \frac{P}{\sqrt{\frac{4}{3}\left(i^2 + ij + j^2\right)}}\sqrt{\frac{\varepsilon_m \varepsilon_d}{\varepsilon_m + \varepsilon_d}} \quad (1)$$

where P is the period of the hole array, ε_m is the dielectric constant of the metal, ε_d is the dielectric constant of the dielectric, and i and j are the scattering orders of the array.[15,16] The sixteen colour plasmonic filter set was designed by scaling the hole size and the array period to shift the resonant wavelength, whilst maintaining similar bandwidths and transmission magnitudes. It is possible to increase the transmission magnitude by using larger holes or a thinner metal, however this also results in an increased bandwidth.[16] A cross section of the simulated plasmonic filter structure is shown in **Figure 1**a; the simulation region (enclosed by a solid purple line) and the unit cell (enclosed by a dashed purple line) are shown in Figure 1b.

The MM component geometry was inspired by an established THz MM absorber.[31] The constituent materials and layer thicknesses were altered to optimise the MM absorber for integration with optical plasmonics. The designed MM absorber consisted of a 150 nm aluminium ground plane and a 150 nm hollow cross aluminium ERR, separated by a 3 μm silicon dioxide spacer. Silicon dioxide was chosen as the dielectric spacer material as it exhibits low loss at optical wavelengths and aluminium was chosen because it exhibits high conductivity at THz frequencies whilst still being sufficiently low loss at optical wavelengths to be used for optical plasmonics filters. A cross-section of the optimised MM absorber unit cell of the SMM is shown in Figure 1c and a top down view is shown in Figure 1d. The hollow cross ERR geometry is as follows: A = 20 μm, B = 5 μm, C = 10 μm, D = 26 μm and the repeat period, M = 27 μm. The SMM uses plasmonic filters patterned into the ground plane of the MM absorber. The MM absorber unit cell that was simulated is as is shown in Figure 1c-d, but with an unperforated ground plane. The absorption spectrum, $A(\omega)$, was calculated using Equation (2):

$$A(\omega) = 1 - R(\omega) - T(\omega) \quad (2)$$

where $R(\omega)$ is the reflection spectrum and $T(\omega)$ is the transmission spectrum, as determined by simulations.[27]

The procedure for fabricating the SMM is outlined at the end of the article. The MM absorber ground plane consisted of sixteen plasmonic filters. Each filter was 1 mm × 1 mm in size and was separated from neighbouring filters by 0.33 mm; the sixteen filters extended to a square area of 5 mm × 5 mm. The hole diameters of each of the filter arrays were measured prior to deposition of silicon dioixde on to the ground plane. A SEM image of a red plasmonic filter (P = 430 nm) is shown in **Figure 2**a,b.

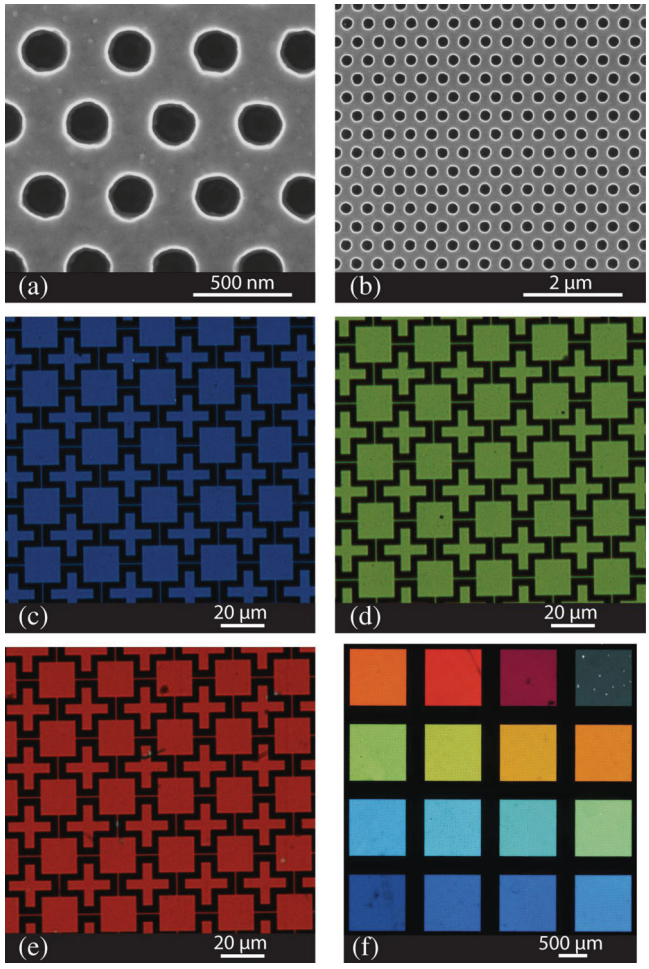

Figure 2. Scanning electron micrographs of a plasmonic filter hole array and transmission microscope images of a synthetic multi-spectral material (SMM). (a)-(b) Scanning electron micrographs of a red plasmonic filter (P = 430 nm) at different magnifications. Transmission microscope images showing electric ring resonators (ERRs) above (c) a blue plasmonic filter (P = 250 nm), (d) a green plasmonic filter (P = 340 nm) and (e) a red plasmonic filter (P = 410 nm). (f) Tessellated transmission microscope image of the region of the SMM covered with plasmonic filters. The ERRs are not visible in this image, however they result in a decrease in intensity of the plasmonic filter transmission spectra.

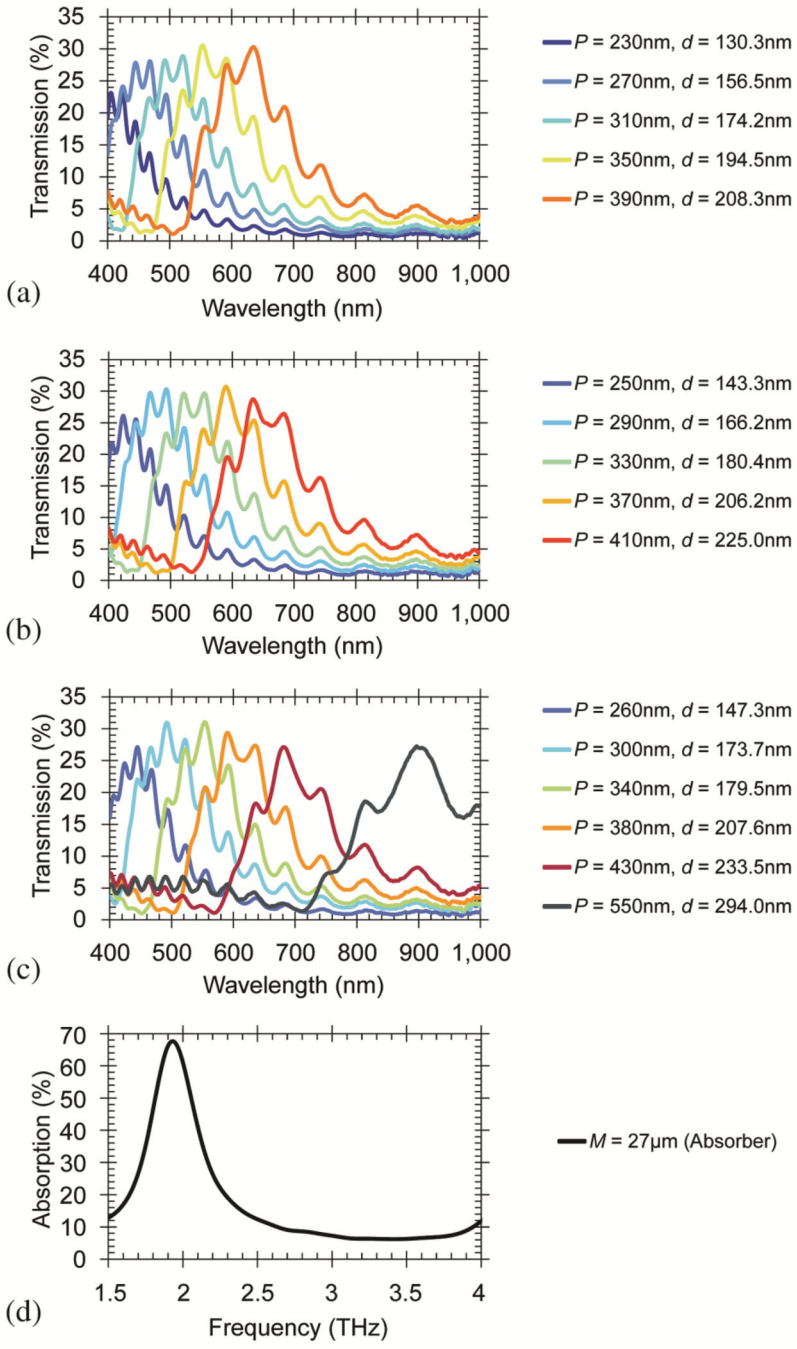

Figure 3. Measured spectral characteristics of the synthetic multispectral material (SMM). The transmission spectra associated with the plasmonic filters are shown in (a)-(c). The hole period, *P*, and hole diameters, *d*, as measured using the scanning electron microscope (SEM) are shown in the legend. (d) Absorption spectrum of the terahertz (THz) metamaterial (MM) component of the SMM. *M* is the period of the MM absorber unit cell.

The ERR array that was patterned after silicon dioxide deposition covered an area of 12 mm × 12 mm over the plasmonic filters.

Transmission microscope images of the completed SMM are shown in Figure 2c–f. Figure 2c–e show the ERR array above blue, green and red plasmonic filter ground plane sections, respectively. Figure 2f shows a tessellated picture of the SMM surface. The ERR structures are not resolved in Figure 2f.

The spectral characteristics of the SMM were investigated in detail using sources and detectors appropriate to the wavelengths of interest and the measurement procedure is described in the experimental section at the end of the article. The transmission spectra from the plasmonic filter regions of the SMM are shown in **Figure 3**a–c. The legend denotes the hole period and the measured hole diameters of each filter. Fabry-Perot oscillations appear in the transmission spectra due to the silicon dioxide dielectric spacer. The peaks are consistent over all colour filters and correspond to a 3 μm resonator cavity with refractive index: $n = 1.48$.[34] The transmission and reflection spectra of the SMM at THz frequencies were measured and, using Equation (2), it was possible to calculate the absorption spectrum, as is shown in Figure 3d. It was observed that the MM absorber component of the SMM exhibits 67% absorption at 1.93 THz.

Our transmission measurements have been made over a large area and we observe a drop in light intensity over the visible range due to the ERR array. The ERR geometry and plasmonic filter positioning can be optimised to maximise the filtered light transmitted over a desired region, whilst still retaining frequency selective THz absorption of the MM component of the SMM. The reduction in transmission magnitude due to the ERRs can be quantified and accounted for by scaling the transmission spectra with respect to the ERR metal fill factor on the surface of the SMM (33.6%), thereby approximating the standalone plasmonic filter spectra. The scaled spectra for three of the plasmonic filter on the SMM, and the corresponding simulation results, are shown in **Figure 4**a. Palik aluminium and silicon dioxide models were used to classify the simulated materials.[35] It should be noted that the simulated structure only used a 200 nm cap layer and therefore did not exhibit Fabry–Pérot oscillations in this wavelength range.

The measured absorption spectra from the SMM and from a MM absorber of the same design, but without a perforated ground plane, are shown in Figure 4b. It can be observed that both structures exhibit similar spectral characteristics in this frequency range, thereby demonstrating the negligible impact that the plasmonic filters have on the MM response. Simulations of the MM absorber were repeated to account for the optical properties of the fabricated materials. The silicon dioxide layer was modelled using the complex

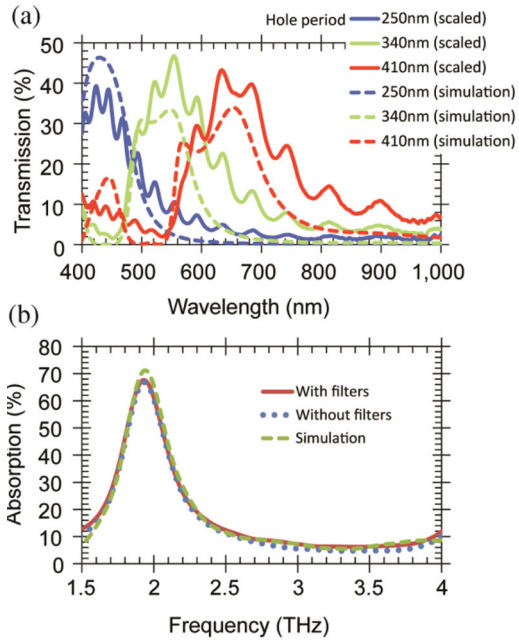

Figure 4. Experimental and simulated spectral characteristics of the synthetic multi-spectral material (SMM). (a) Experimentally measured transmission spectra from the blue, green and red plasmonic filters sections of the SMM, scaled to account for the presence of the electric ring resonators (ERRs). Also shown is the simulated transmission spectra for the same periods and hole sizes for standalone filters with a 200 nm cap layer. (b) Experimentally measured terahertz (THz) absorption spectra of the SMM compared with a standalone metamaterial (MM) absorber of the same design, but without a perforated ground plane. Also shown are the simulation results for the standalone, unperforated MM absorber.

refractive index: $n = 2.04 + i0.16$ and refractive index parameters, defined by Rakić,[36] were used to characterise the aluminium at THz frequencies. The observed simulated absorption magnitude of 71.2% at 1.94 THz is in good agreement with the measured SMM absorption spectrum. The simulation results imply that the silicon dioxide we have deposited has a higher absorption coefficient than has previously been documented.[37]

In this article we have demonstrated the design, fabrication and characterisation of a new type of multi-spectral material that hybridises optical plasmonic filters with a THz MM absorber to combine multiple functionalities as well as multi-spectral capabilities into a single material. Our device exhibits multiple functionalities by combining the THz absorber material within the colour filter structure and therefore eliminates the need for a separate material for THz detection.

We have fabricated a SMM that combines fifteen colour plasmonic filters, a single NIR plasmonic filter and a frequency selective THz MM absorber. Our device demonstrates that the presence of plasmonic filter hole arrays in a THz MM absorber ground plane have negligible impact on the THz absorption spectrum associated with the MM.

The plasmonic filters can be used in conjunction with photodiodes and the THz MMs can be combined with a detector material, for example a microbolometer, therefore demonstrating a clear path for integrating a multi-spectral material with a CMOS imaging chip to create a multi-spectral camera. SMMs have the potential to maximise the spectral information density of an optical system. By using a single material with multiple engineered optical properties over the same surface area we open up the possibility of creating high resolution multi-spectral imagers.

Experimental Section

Electromagnetic Simulations: The plasmonic filter simulations are set up as follows: a 150 nm aluminium layer was placed between a semi-infinite silicon dioxide layer and a 200 nm silicon dioxide cap layer. The aluminium was patterned with two glass holes and the silicon dioxide cap layer was patterned with two etch holes to account for the cap layer topography after deposition of silicon dioxide. A mesh grid with a maximum cell size of 5 nm was defined in the vicinity of the holes. Symmetric and anti-symmetric boundary conditions were used to form the triangular hole array structure, and perfectly matched layers (PML) were used in the *z* boundaries. The aluminium surface was illuminated by a 400 nm to 1 µm plane-wave source and the transmission spectra were recorded by a monitor placed on the opposite side of the aluminium.

A similar simulation method was used for the MM absorber in which the structure was illuminated from above by a plane-wave source. Symmetric and anti-symmetric boundary conditions were once again used in *x* and *y*; PML boundary conditions were used in the *z*-direction. The maximum mesh step size in the region of the MM was 75 nm in *x* and *y*, and 25 nm in *z*. Reflection and transmission monitors were placed above and below the MM unit cell, respectively.

Fabrication of the Synthetic Multi-Spectral Material: The plasmonic filter ground plane was fabricated by evaporating a 150 nm aluminium film on to a glass slide. 50 nm of silicon nitride was deposited on to the aluminium to improve the adhesion of spin coated ZEP520A electron beam resist with the material surface. The sixteen colour plasmonic filters were patterned into the resist using a Vistec VB6 electron beam lithography (EBL) tool. The nanohole patterns were developed in o-xylene at 23 °C for 35 s and were etched using standard dry etch processing. The silicon nitride layer was etched using trifluoromethane / oxygen (CHF_3/O_2) in an Oxford Instruments RIE80+ and the aluminium was etched using silicon tetrachloride ($SiCl_4$) in an Oxford Instruments RIE100. The ZEP520A and silicon nitride mask were then removed from the aluminium surface. The sample was then cleaned and 3 µm of silicon dioxide was deposited on top of the aluminium layer using plasma enhanced chemical vapour deposition (PECVD). As the plasmonic filters are unaltered for use as a ground plane in the SMM, the fabrication procedure outlined here can be used to make standalone plasmonic filters.[16,20]

The SMM was completed by fabricating the ERR array on the silicon dioxide surface. Fabrication of the ERR array was carried out by spin coating a bilayer of poly(methyl methacrylate) (PMMA) on to the silicon dioxide surface. EBL was used to define features in the PMMA and the PMMA was developed using isopropyl alcohol: methyl isobutyl ketone (IPA: MIBK). A 150 nm layer of aluminium was deposited on top of the device and a lift off process utilising hot acetone was used to remove the remaining resist and unwanted aluminium.

Experimental Characterization of the Synthetic Multi-Spectral Material: The optical and NIR spectra from the plasmonic filter sections of the SMM were measured using a TFProbe MSP300 microspectrophotomer with a white light halogen lamp source and a detector with a spot size of 100 µm. The transmission spectra were normalised to the white light source.

Characterisation of the MM absorber component of the SMM was performed using a Bruker IFS 66v/S Fourier transform infrared spectrometer (FTIR). The sample was illuminated by a mercury arc lamp and the transmission spectrum at normal incidence, $T(\omega)$, and reflection spectrum at 30°, $R(\omega)$, were measured. The transmission spectrum was

normalised to a 7 mm open aperture and the reflection spectrum was normalised to a gold mirror through a 10 mm aperture. The source aperture had a diameter of 12 mm and 4 mm for the transmission and reflection measurements, respectively.

Acknowledgements

The authors would like to thank the staff of the James Watt Nanofabrication Centre at the University of Glasgow for help in fabricating the devices reported in this paper. This research was funded from EPSRC grants EP/I017461/1 and EP/J018678/1.

Received: October 2, 2013
Revised: November 5, 2013
Published online: November 27, 2013

[1] T. May, G. Zieger, S. Anders, V. Zakosarenko, H.-G. Meyer, M. Schubert, M. Starkloff, M. Rößler, G. Thorwirth, U. Krause, *Proc. SPIE* **2009**, *7309*, 73090E.
[2] M. Kowalski, M. Piszczek, N. Palka, M. Szustakowski, *Proc. SPIE* **2012**, *8544*, 85440N.
[3] S. G. Kong, J. Heo, F. Boughorbel, Y. Zheng, B. R. Abidi, A. Koschan, M. Yi, M. A. Abidi, *Int. J. Comput. Vis.* **2007**, *71*, 215.
[4] A. L. Chan, S. R. Schnelle, *Opt. Eng.* **2013**, *52*, 017004.
[5] S. M. Sze, *Semiconductor Devices: Physics and Technology*, Wiley, New York **2002**.
[6] F. Niklaus, C. Vieider, H. Jakobsen, *Proc SPIE* **2007**, *6836*, 68360D.
[7] A. W. M. Lee, B. S. Williams, S. Kumar, Q. Hu, J. L. Reno, *IEEE Photon. Technol. Lett.* **2006**, *18*, 1415.
[8] J. Grant, I. Escorcia-Carranza, C. Li, I. J. H. McCrindle, J. Gough, D. R. S. Cumming, *Laser Photon. Rev.* **2013**, DOI:10.1002/lpor201300087.
[9] M. Perenzoni, N. Massari, S. Pocas, J. Meilhan, F. Simoens, IRMMW-THz Conference 2010, Rome, 5–10 September, **2010**.
[10] M. Perenzoni, N. Massari, D. Stoppa, S. Pocas, B. Delplanque, J. Meilhan, F. Simoens, W. Rabaud, ESSCIRC Conference 2012, Bordeaux, 17–21 September, **2012**.
[11] I. J. H. McCrindle, J. Grant, T. D. Drysdale, D. R. S. Cumming, *Opt. Express* **2013**, *21*, 19142.
[12] T. W. Ebbesen, H. J. Lezec, H. F. Ghaemi, T. Thio, P. A. Wolff, *Nature* **1998**, *391*, 667.
[13] H. F. Ghaemi, T. Thio, D. E. Grupp, T. W. Ebbesen, H. J. Lezec, *Phys. Rev. B* **1998**, *58*, 6779.
[14] W. L. Barnes, A. Dereux, T. W. Ebbesen, *Nature* **2003**, *424*, 824.
[15] C. Genet, T. W. Ebbesen, *Nature* **2007**, *445*, 39.
[16] Q. Chen, D. R. S. Cumming, *Opt. Express* **2010**, *18*, 14056.
[17] D. Inoue, A. Miura, T. Nomura, H. Fujikawa, K. Sato, N. Ikeda, D. Tsuya, Y. Sugimoto, Y. Koide, *Appl. Phys. Lett.* **2011**, *98*, 093113.
[18] K. Walls, Q. Chen, S. Collins, D. R. S. Cumming, T. D. Drysdale, *IEEE Photon. Technol. Lett.* **2012**, *24*, 602.
[19] Q. Chen, D. Chitnis, K. Walls, T. D. Drysdale, S. Collins, D. R. S. Cumming, *IEEE Photon. Technol. Lett.* **2012**, *24*, 197.
[20] Q. Chen, D. Das, D. Chitnis, K. Walls, T. D. Drysdale, S. Collins, D. R. S. Cumming, *Plasmonics* **2012**, *7*, 695.
[21] Y. Huo, C. C. Fesenmaier, P. B. Catrysse, *Opt. Express* **2010**, *18*, 5861.
[22] P. B. Catrysse, B. A. Wandell, *J. Opt. Soc. Am. A* **2003**, *20*, 2293.
[23] J. B. Pendry, A. J. Holden, W. J. Stewart, I. Youngs, *Phys. Rev. Lett.* **1996**, *76*, 4773.
[24] J. B. Pendry, A. J. Holden, D. J. Robbins, W. J. Stewart, *IEEE Trans. Microw. Theory Tech.* **1999**, *47*, 2075.
[25] W. J. Padilla, M. T. Aronsson, C. Highstrete, M. Lee, A. J. Taylor, R. D. Averitt, *Phys. Rev. B* **2007**, *75*, 041102.
[26] P. R. West, S. Ishii, G. V. Naik, N. K. Emani, V. M. Shalaev, A. Boltasseva, *Laser Photon. Rev.* **2010**, *4*, 795.
[27] N. I. Landy, S. Sajuyigbe, J. J. Mock, D. R. Smith, W. J. Padilla, *Phys. Rev. Lett.* **2008**, *100*, 207402.
[28] N. I. Landy, C. M. Bingham, T. Tyler, N. Jokerst, D. R. Smith, W. J. Padilla, *Phys. Rev. B* **2009**, *79*, 125104.
[29] H. Tao, N. I. Landy, C. M. Bingham, X. Zhang, R. D. Averitt, W. J. Padilla, *Opt. Express* **2008**, *16*, 7181.
[30] H. Tao, C. M. Bingham, A. C. Strikwerda, D. Pilon, D. Shrekenhamer, N. I. Landy, K. Fan, X. Zhang, W. J. Padilla, R. D. Averitt, *Phys. Rev. B* **2008**, *78*, 241103.
[31] J. Grant, Y. Ma, S. Saha, L. B. Lok, A. Khalid, D. R. S. Cumming, *Opt. Lett.* **2011**, *36*, 1524.
[32] J. Grant, Y. Ma, S. Saha, A. Khalid, D. R. S. Cumming, *Opt. Lett.* **2011**, *36*, 3476.
[33] Lumerical finite difference time domain (FDTD) Solutions. http://www.lumerical.com, accessed: September, **2013**.
[34] F. A. Jenkins, H. E. White, *Fundamentals of Optics*, McGraw-Hill, New York **1981**.
[35] E. D. Palik, *Handbook of Optical Constants of Solids*, Volumes I, II, and III, Academic Press, New York **1985**.
[36] A. D. Rakić, *Appl. Opt.* **1995**, *34*, 4755.
[37] M. Naftaly, R. E. Miles, *J. Appl. Phys.* **2007**, *102*, 043517.